IRSTI 29.19.31 https://doi.org/10.26577/phst2024v11i2b06

Auto-oscillations of current in injection structures p+-p (Si<Mn>) based on heavily compensated silicon

K.S. Ayupov[1], H.F. Zikrillaev[1], E.B. Saitov[2]*, N.U. Abdullaeva[3], Z.N. Umarkhojayeva[1] and M.M. Yakhyayev[1]

[1]Tashkent State Technical University, Tashkent, 100095, Uzbekistan
[2]University of Tashkent for Applied Sciences, Str. Gavhar 1, Tashkent 100149, Uzbekistan
[3]Tashkent regional branch of Astrakhan State Technical University. Tashkent 100164, Uzbekistan
4Tashkent Medical Academy, Tashkent 100095, Uzbekistan
*e-mail: elyor.saitov@utas.uz
(Received May,21, 2024; received in revised form November 20,2024; accepted November 28, 2024)

This paper presents the findings of a study on the current-voltage characteristics (IVC) and current self-oscillations in n++-p(Si)-p+ structures made from heavily compensated silicon. We observed that the self-oscillations in manganese-doped silicon are linked to the injection of holes. During our examination of the I-V characteristics in p*-p(Si)-p* structures, we discovered that certain voltage levels can trigger self-oscillations in injection current, which are related to unipolar hole injection. Moreover, these current self-oscillations consistently promote vertical current growth within the IVC region. Initially, before stabilizing into fixed current self-oscillations, we noted chaotic fluctuations that transitioned to regular oscillations with a slight increase in voltage. We identified the characteristics of highly compensated silicon in an extremely nonequilibrium state and highlighted the unique functional capabilities of this material, which differ from those of conventional semiconductors. This discovery paves the way for developing innovative types of photoelectric, optoelectrical, and magnetoelectrical devices, as well as sensors for physical parameters and classical semiconductor devices that demonstrate high resistance to radiation and thermal effects.

Key words: silicon, current, injection, structure, compensation, self-oscillations, hole, trap.
PACS number(s): -61.72.jd.

1. Introduction

The modern development of electronics and microelectronics would be unimaginable without advancements in the contact properties of semiconductor devices [1, 2]. This necessitates the formulation of various contact types, such as ohmic, injection, or barrier contacts, each with specific parameters, optimized technological processes, and reduced production costs [3-5]. To achieve this, technologies are being developed to replace expensive materials, such as gold and silver, with more affordable alternatives. In this context, the aim is to align laboratory technologies for producing contacts in semiconductor devices with factory conditions. Many physical effects and phenomena remain underutilized due to the limitations of current technological methods in large-scale semiconductor device production.

The study of injection currents in compensated semiconductors, particularly in silicon that contains impurity atoms with deep energy levels, provides valuable insights into the nature of these levels and the physical mechanisms underlying current flow [6]. The analysis of current-voltage (I-V) characteristics of such structures enables researchers to determine the injection properties and potential barrier heights that arise at contact boundaries. This evaluation is crucial for assessing the influence of injection contacts on the observed physical effects [7, 8]. In this regard, structures based on compensated silicon are of considerable interest to researchers, as they display several intriguing physical phenomena that could have wide-ranging applications in semiconductor electronics.

Developing p^+-p-p^+ and n^+-n-n^+ structures based on compensated silicon presents significant challenges. For instance, when fabricating structures

from compensated silicon doped with atoms such as Mn, Zn, or S, thermal processing is necessary, which can alter the material's electrophysical properties [9-13]. Moreover, forming these contacts through melting various alloys or using diffusion techniques is not feasible due to the high diffusion coefficients of the materials typically used for contacts. To overcome this limitation, we have adopted an unconventional technological approach to create injection contacts. This method not only enables the formation of injection contacts but also brings the production technology closer to standard factory conditions.

2. Materials and methods for obtaining injection structures

To create injection contacts, industrial-grade silicon wafers, designated KDB-2 and KDB-10 (boron-doped dislocation silicon), with a diameter of 76 mm were selected as the starting material. The silicon was sliced into wafers with a thickness of 1 mm, followed by mechanical grinding to eliminate the damaged surface layer. This grinding process used a suspension of silicon carbide, grade M-14, and approximately 100 μm was removed from each side of the wafer.

After polishing and a preliminary chemical cleaning, the diffusion of boron or phosphorus impurity atoms was carried out under factory conditions. The diffusion of boron and phosphorus in silicon was executed in two stages using solid sources. Boron nitride (BN) and phosphorus pentoxide (P_2O_5) served as the diffusing agents. The initial boron diffusion was performed at a temperature of 1353 K for 40 minutes in a nitrogen atmosphere to develop an enriched layer. As is well known, BN is stable and prevents the oxidation of the source, leading to the formation of boron oxide (B_2O_3) on the silicon wafer. This method results in a high concentration of boron in silicon, achieving a doping uniformity of approximately 5%. Following the initial diffusion, boron atoms were further diffused at a temperature of 1473 K for 6.5 hours in a nitrogen atmosphere. The thickness of the resulting p+-layers varied from a few micrometers to 30-40 μm, depending on the diffusion temperature and duration.

To create n-type contacts, P_2O_5 was utilized as the diffusant. Phosphorus diffusion was carried out in a nitrogen atmosphere at a temperature of 1393 K for 40 minutes, followed by additional diffusion at 1473 K. By carefully controlling the diffusion time, we achieved an n+ injection layer with a thickness ranging from a few microns to 35-40 μm, with a doping uniformity of ±5%.

The solid sources BN and P_2O_5 create diffusion layers within silicon wafers that exhibit a high surface concentration, $N_s = 10^{20}$ cm^{-3}. In our experiments, surface resistivity measurements indicated that the boron and phosphorus concentrations were approximately $N_s \approx 10^{19}$ cm^{-3}. This level of concentration was influenced by lower temperatures and relatively short diffusion durations.

To fabricate structures based on compensated silicon doped with manganese impurity atoms, a gas-phase diffusion method was employed. For doping purposes, the p^+-p-n^+ and n^+-p-n^+ structures were cut into parallelepiped crystals measuring (1-10) x (1-5) x 0.8 mm³. To remove mechanical defects, the crystals were ground on four sides while leaving the injection layer intact, followed by chemical etching. Subsequently, these structures were placed in quartz ampoules along with a manganese diffusant. The ampoules were evacuated to a vacuum of about 10^{-5} mmHg before being sealed. The diffusion annealing of the structures was conducted in a vacuum tube furnace at 1973°C, which allowed for temperature control with an accuracy of ±1 K. Table 1 presents the parameters of the resulting p^+-p-ρ^+ structures, which were dependent on the diffusion conditions of the manganese impurity atoms.

Table 1 – Diffusion process conditions and parameters of the obtained structures

№	T, K	D см^2/sec	t, hour	N_p^+,cm^{-3}	N_p,cm^{-3}, base	N_p^+,cm^{-3}
1.	1473	$5{,}1\cdot10^{-12}$	1	$2{,}2\cdot10^{16}$	$1{,}5\cdot10^{15}$	$2{,}2\cdot10^{16}$
2.	1473	$5{,}1\cdot10^{-12}$	2	$2{,}36\cdot10^{17}$	$1{,}5\cdot10^{15}$	$2{,}36\cdot10^{17}$
3.	1473	$5{,}1\cdot10^{-12}$	3	$2{,}3\cdot10^{18}$	$1{,}5\cdot10^{15}$	$2{,}3\cdot10^{18}$
4.	1473	$5{,}1\cdot10^{-12}$	4	$3{,}7\cdot10^{18}$	$1{,}5\cdot10^{15}$	$3{,}7\cdot10^{18}$
5.	1473	$5{,}1\cdot10^{-12}$	6	$3{,}4\cdot10^{19}$	$1{,}5\cdot10^{15}$	$3{,}4\cdot10^{19}$

Continuation of the table

№	T, K	D см^2/sec	t, hour	N_p^+,cm^{-3}	N_p,cm $^{-3}$, base	N_p^+,cm^{-3}
6.	1473	$5{,}1\cdot10^{-12}$	10	$9{,}5\cdot10^{19}$	$1{,}5\cdot10^{15}$	$9{,}5\cdot10^{19}$
7.	1473	$5{,}1\cdot10^{-12}$	12	$1{,}26\cdot10^{20}$	$1{,}5\cdot10^{15}$	$1{,}26\cdot10^{20}$
8.	1473	$5{,}1\cdot10^{-12}$	15	$2{,}0\cdot10^{20}$	$1{,}5\cdot10^{15}$	$2{,}0\cdot10^{20}$
9.	1473	$5{,}1\cdot10^{-12}$	17	$2{,}6\cdot10^{20}$	$1{,}5\cdot10^{15}$	$2{,}6\cdot10^{20}$
10.	1473	$5{,}1\cdot10^{-12}$	20	$3{,}41\cdot10^{20}$	$1{,}5\cdot10^{15}$	$3{,}41\cdot10^{20}$
11.	1473	$5{,}1\cdot10^{-12}$	24	$3{,}6\cdot10^{20}$	$1{,}5\cdot10^{15}$	$3{,}6\cdot10^{20}$
12.	1473	$5{,}1\cdot10^{-12}$	30	$4{,}2\cdot10^{20}$	$1{,}5\cdot10^{15}$	$4{,}2\cdot10^{20}$
13.	1473	$5{,}1\cdot10^{-12}$	40	$4{,}9\cdot10^{20}$	$1{,}5\cdot10^{15}$	$4{,}9\cdot10^{20}$

The diffusion temperature was monitored using a thermocouple placed directly next to the quartz ampoule. This setup allowed for precise control over the manganese diffusion temperature in silicon, which is crucial for defining the various diffusion technological modes. Such control facilitates the development of a reproducible technology for producing structures based on silicon that is compensated with manganese impurity atoms.

To differentiate compensating impurities from various uncontrolled defects, control samples were simultaneously annealed under the same technological conditions. The high diffusion coefficient of manganese impurity atoms in silicon enabled uniform doping of the structure bases within a short annealing time. This approach effectively prevents the deep penetration of boron or phosphorus impurity atoms into the silicon.

Table 2 – The parameters of the obtained structures depending on the diffusion temperature of manganese impurity atoms in silicon.

The brand of the initial sample	The concentration of boron $N\cdot10^{16}$, cm^{-3}	Diffusion temperature - °C	Diffusion time, t	Type of conductivity of the base after diffusion	Sheet resistance of the base after diffusion ρ, Ω·cm	Mobility μ, cm^2/B·sec
1	2	3	4	5	6	7
CDB-2	1,7	1100	1,5	p	$6{,}3\cdot10^3$	230
CDB-2	1,7	1130	1,5	n	$2{,}0\cdot10^5$	970
CDB-7,5	0,3	1080	1,5	p	$7{,}0\cdot10^4$	184
CDB-7,5	0,3	1110	1,5	n	$6{,}0\cdot10^4$	1010
CDB-10	0,2	1030	1,5	p	$8{,}0\cdot10^2$	196
CDB-10	0,2	1035	1,5	p	$3{,}6\cdot10^3$	208
CDB-10	0,2	1040	1,5	p	$7{,}4\cdot10^4$	200
CDB-10	0,2	1045	1,5	p	$1{,}4\cdot10^5$	195
CDB-10	0,2	1050	1,5	n	$1{,}5\cdot10^5$	980
CDB-10	0,2	1060	1,5	n	$7{,}1\cdot10^4$	910
CDB-10	0,2	1080	1,5	n	$2{,}8\cdot10^4$	1020

By controlling the diffusion temperature, we were able to obtain structures with bases that exhibited both hole and electron conductivity, each with varying resistivity values. This process resulted in the production of structures such as p^+-p(Si)-p, p^+-n(Si)-p^+, n^+-p(Si)-n^+, and n^+-n(Si)-n^+. Once the diffusion process was completed, we ground the surfaces of the samples to 100 μm on all four sides. This was done to remove the enriched layer of manganese atoms, except on the sides where the specially created injection layers were located. The resistivity of the bases of these structures was measured through conductivity assessments while obtaining the voltage-current characteristics (I-V characteristics).

3. Results and discussion

The I-V characteristics of the structures were investigated in darkness at room temperature. The study revealed a sharp increase in current at certain applied voltage values. To elucidate the mechanism

of current conduction in the injection structures and demonstrate that this increase is associated with unipolar injection, we examined the I-V characteristics of the initial samples KDB-2; 10 before and after thermal annealing, as well as structures with injection contacts and control samples (see Fig. 1). Additionally, for comparison, we investigated current conduction in injection structures that were compensated with manganese impurity atoms.

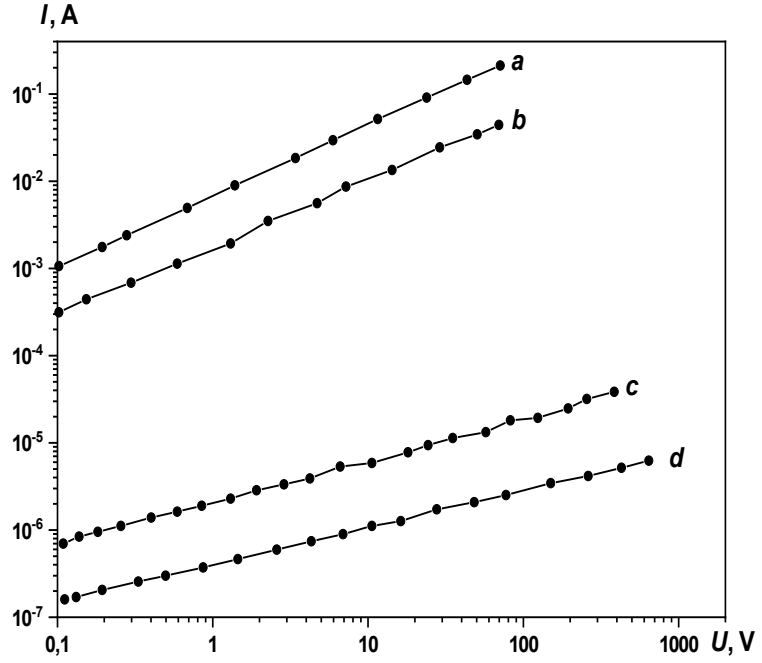

Figure 1 – The I-V characteristics of the initial and control annealed structures of p^+-p-p^+ at a temperature of 300 K in darkness: a) p^+ -p- p^+ before annealing; b) p^+-p-p^+ after annealing; c) KDB before annealing; d) KDB after annealing.

To confirm that the sharp increase in current is indeed related to the unipolar injection of holes, we examined the I-V characteristics of several structures: p^+-p(Si)-p^+, p^+-n(Si)-p^+, n^+-p(Si)-n^+, and n^+-n(Si)-n^+, all based on compensated silicon doped with manganese (see Figure 2). These investigations showed that unipolar injection of holes specifically occurs in the p^+-p(Si)-p^+ structures, which are responsible for the emergence of current injection instabilities.

The I-V characteristics of the structures were assessed under dark conditions and at room temperature. Our analysis revealed a sharp increase in current at specific voltage values. To demonstrate that this increase is linked to unipolar injection, we evaluated the I-V characteristics of the initial samples KDB-2 and KDB-10, both before and after thermal annealing, as well as in structures containing manganese impurity atoms and control samples (see Fig. 2). A comparison of the obtained I-V characteristics confirmed that the sharp increase in current is indeed associated with the injection of charge carriers into the base of the structures doped with manganese impurity atoms. In contrast, other structures (see Fig. 2 curves 2, 3, 4) did not exhibit such a sharp increase in current.

To demonstrate that the sharp increase in current is specifically related to the unipolar injection of holes, we investigated the I-V characteristics of various structures: p^+-p(Si)-p^+, p^+-n(Si)-p^+, n^+-p(Si)-n^+, and n^+-n(Si)-n^+. These structures are based on compensated silicon doped with manganese impurity atoms (see Fig. 2, curve 1). Our studies revealed that unipolar injection of holes occurs predominantly in the p^+-p(Si)-p^+ structures, which contribute to the emergence of current injection instabilities.

The examination of the I-V characteristics of these injection structures with varying concentrations in the injecting layer allowed us to identify the specific boron concentration at which the sharp increase in current is observed. The I-V characteristics from these investigations are illustrated in Fig.

3. As shown in the figure, an increase in boron concentration in the injecting layer, within the range of $N_B=10^{15}$ to 10^{20} cm^{-3}, leads to a rise in current when the concentration of boron atoms reaches approximately 10^{17} cm^{-3} or higher.

It is important to note that the increase in boron concentration in the p+-layer results in a shift towards lower voltages, where the degree of current increase becomes noticeable. At concentrations below $N_B \leq 10^{17} cm^{-3}$, there is no significant effect on the I-V characteristics in the p^+–p(Si)–p^+ structures. However, at injecting contact concentrations of $N_B=10^{17}$ cm^{-3} to 10^{20} cm^{-3}, after the sharp increase in current, oscillations in the circuit current start to appear.

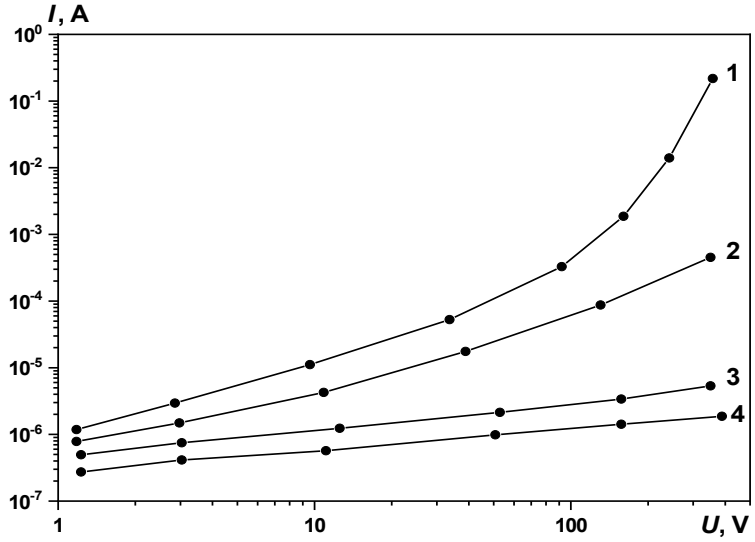

Figure 2 – I-V characteristics of the structures: curve 1: p^+-p(Si<Mn>)p^+; curve 2: p^+-n(Si<Mn>)-p^+; curve 3: n^+-n(Si<Mn>); curve 4: n^+-p(Si<Mn>)-n^+.

At a temperature of 300 K, the specific resistance of the base measured $\rho = 5 \times 10^4$ Ω·cm. Analyzing the voltage-current characteristics of the p^+-p(Si)-p^+ structures provided valuable insights into unipolar hole injection. According to existing literature [14-20], unipolar carrier injection occurs in semiconductor materials that contain deep energy levels, which serve as traps for the primary charge carriers.

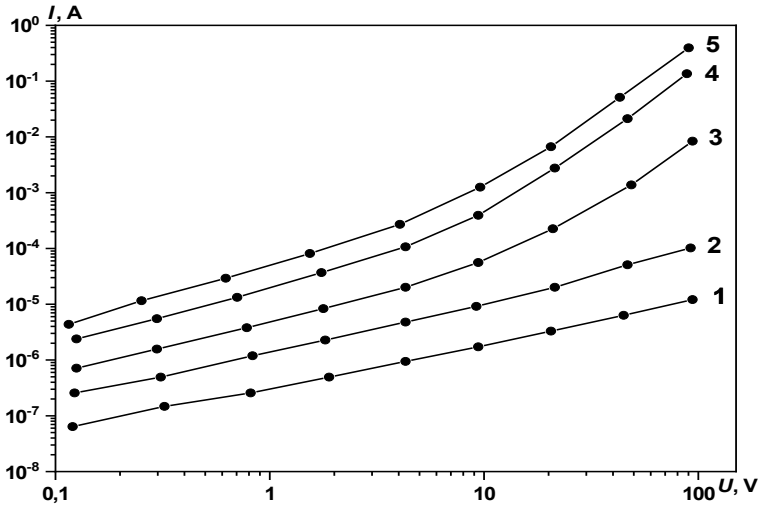

Figure 3 – I-V characteristics of p^+-p(Si<Mn>)-p^+ structures with different concentrations of p^+ layer: curve 1 – 10^{15} cm^{-3}; curve 2 – 10^{16} cm^{-3}; curve 3 – 10^{17} cm^{-3}; curve 4 – 10^{18} cm^{-3}; curve 5 – 10^{19} cm^{-3} at T=300K

The quadratic section of the I-V characteristics of the structures corresponds to the monopolar injection of holes. The voltage at which the sharp increase in current begins, known as V_{fct} (where 'fct' stands for field charge of traps), indicates the point at which the traps are fully charged. This allows for a clear determination of the complete filling of the energy level of the manganese impurity atom by these traps, which are responsible for the excitation of current oscillations in the studied structure. The results from the I-V characteristic studies of the structures at various illumination intensities provide valuable information regarding the total concentration and ionization energy of the manganese impurity atoms in compensated silicon.

If the value of V_{fct} is known, the concentration of impurity atoms at the energy level can be determined using the appropriate formula:

$$N_t = \frac{\varepsilon V_{fct}}{ed^2} \quad (1)$$

where ε is dielectric constant of silicon, e is charge of the electron, d is thickness of the base of the structures. This, in turn, allows for the determination of the ionization energy from the energy equation at a given temperature.

$$E_v - E_t = kT\, ln \frac{N_S}{QgN_t} \quad (2)$$

where Q is a coefficient, which shows the ratio of the concentration of free charge carriers to the concentration of carriers trapped at energy levels, is defined by the expression:

$$Q = \frac{n_0 L^2}{\varepsilon V_X} \quad (3)$$

The calculation results show that for compensated silicon doped with manganese impurity atoms, this value is approximately Q ≈ (1 to 3)$^{(1/2)}$ 10, while the maximum values of concentration and activation energy of the manganese level are $N_t = 2.4 \times 10^{10}$ cm^{-3} and Et = (0.14 to 0.16) eV, respectively. Knowing the experimental values of V_{fct} and Q at various light intensities for compensated Si<Mn> samples with different degrees of compensation, it is possible to determine the concentration of the energy level in the structures p^+-p(Si<Mn>)-p^+ that are responsible for the excitation of current oscillations.

The results from the I-V characteristics studies allow us to determine the mobility of charge carriers. This mobility is a crucial parameter for understanding not only the mechanism behind injection instability but also the changes in carrier mobilities under conditions of strong compensation [17]. To calculate the mobility, the following formula was employed:

$$\mu = Id^2/EV \quad (4)$$

The mobility of holes was found to be in the range of μ = 100 to 300 cm²/V·s, depending on temperature, the degree of compensation of the base structures, and light intensity.

The results of the I-V characteristics study conducted on various structures based on compensated silicon revealed that a noticeable sharp increase in current, referred to as the bulk field charge current (BFCC), along with associated current oscillations, is only evident in the p^+-p(Si)-p^+ structures. In contrast, the p^+-n(Si)-p^+, n^+-n(Si)-n^+, and n^+-p(Si)-n^+ structures did not show any signs of BFCC or current oscillations. This suggests that the phenomena observed, particularly the vertical increase in current and the current oscillations, are linked to hole injection into the base of the p^+-p(Si)-p^+ structures.

From the analysis of the literature data [21-25], it is clear that the injection current oscillations in the p^+-p(Si)-p^+ structures are particularly important for gaining additional insights to develop a unified model of current instability in compensated silicon.

The studies on the I-V characteristics of the p^+-p(Si)-p^+ structures demonstrate that injection current oscillations occur at specific voltage levels, which are linked to the unipolar injection of holes. The research findings indicate that current oscillations in these structures are consistently triggered following a vertical increase in current within the I-V characteristic region. Notably, before stable current oscillations are established, chaotic oscillations can be observed. These chaotic oscillations transition into regular oscillations with only a slight increase in voltage. Figure 4 illustrates the various forms of current oscillations.

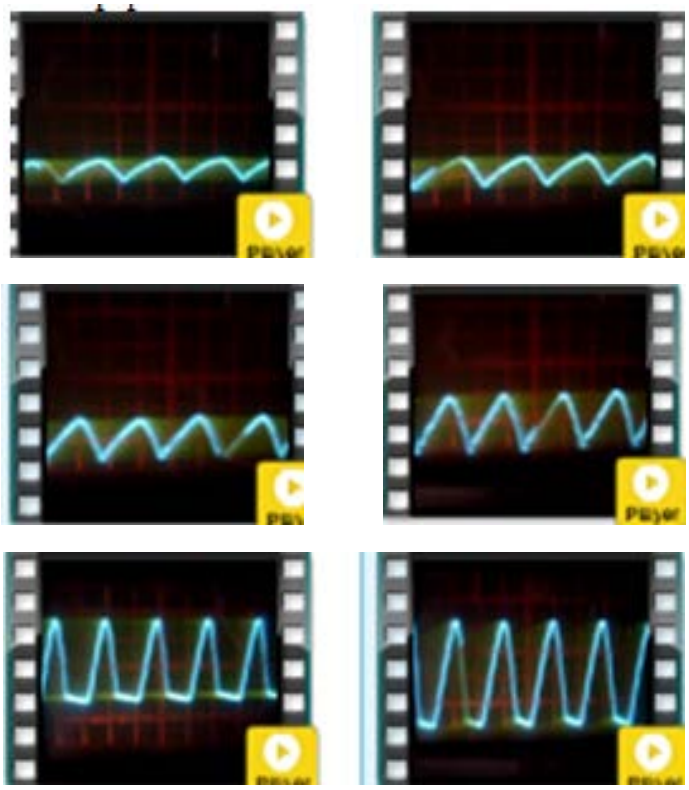

Figure 4 – Forms of injection current oscillations in structures p^+-p(Si<Mn>)-p^+.

To determine the dependence of the conditions for excitation and parameters of current oscillations on the degree of compensation of the base, structures p^+-p(Si<Mn>)-p^+ with base resistivities $\rho_e = 10^2$ to 10^5 Ω•cm was obtained. The studies showed that oscillations in the structures are observed at room temperature and in the dark, starting with base resistivities $\rho_e \geq 3 \cdot 10^2$ Ω•cm.

The research findings demonstrate that injection current self-oscillations in p^+-p(Si)-p^+ structures are observed across a wide range of base resistivity, ranging from 100 to 100,000 Ω•cm. The magnitude of these oscillations depends on the concentration of electroactive manganese dopant atoms. Additionally, it has been established that these injection current self-oscillations exhibit bulk characteristics. The experimental results provide an opportunity to select p^+-p(Si)-p^+ structures with optimal base electrophysical parameters for further investigations.

4. Conclusion

The study of auto-oscillations in p^+-p(Si<Mn>) injection structures, based on heavily compensated silicon, reveals significant insights into the dynamics of current instability. During unipolar injection, within particular voltage intervals, current oscillations are observed. These oscillations are of great significance as they reveal the complex interaction among compensation, base resistivity, and dopant concentration. Notably, as the voltage rises, the oscillations transition from chaotic to regular forms, opening up avenues for a more profound comprehension of their fundamental mechanisms.

Experimental investigations have firmly established that injection current oscillations occur over a wide range of base resistivity, spanning from 10^2 to 10^5 Ω·cm. Moreover, they are strongly influenced by the concentration of manganese atoms. This research emphasizes the bulk nature of these oscillations and their stability at room temperature in the absence of illumination. Consequently, p^+-p(Si<Mn>) structures emerge as a highly promising platform for further exploration and hold potential for applications in semiconductor devices.

The findings not only contribute to the evolution of a unified model of current instabilities in compensated silicon but also lay the groundwork for

optimizing the electrophysical parameters of such structures, thereby advancing semiconductor technologies.

Acknowledgments

The work was financially supported by the Ministry of Innovative Development of the Republic of Uzbekistan within the framework of the project F-OT-2021-497 – "Development of the scientific foundations for the creation of solar cogeneration plants based on photovoltaic thermal batteries.

The authors express their gratitude to the professors of Tashkent State Technical University N.F. Zikrillayev and Kh.M. Iliyuev for his scientific and practical help in writing this article.

References

1. Liu X.F., Xing K., Tang Ch.S., Sun Sh., Chen P., Qi D.-Ch., Breese M. B.H., Fuhrer M.S., Wee A.T.S., Yin X. Contact resistance and interfacial engineering: Advances in high-performance 2D-TMD based devices // Progress in Materials Science. – 2025. -Vol.148. – P.101390. https://doi.org/10.1016/j.pmatsci.2024.101390

2. Kim K. S., Kwon J., Ryu H., Kim Ch., Kim H., Lee E.-K., Lee D., Seo S., Han N. M., Suh J. M., Kim J., Song M.-K., Lee S., Seol M., Kim J. The future of two-dimensional semiconductors beyond Moore's law // Nature Nanotechnology. – 2024. – Vol. 19. – P. 895–906. https://doi.org/10.1038/s41565-024-01695-1

3. Zheng Y., Gao J., Han Ch., Chen W. Ohmic contact engineering for two-dimensional materials // Cell Reports Physical Science. – 2021. – Vol. 2(1). – P. 100298. https://doi.org/10.1016/j.xcrp.2020.100298

4. Pourtois R. D., Houssa G., Afzalian M. A. Fundamentals of low-resistive 2D-semiconductor metal contacts: an ab-initio NEGF study // npj 2D Materials and Applications. – 2023. – Vol.7. -№. 38. https://doi.org/10.1038/s41699-023-00402-3

5. Kao K. C. Charge carrier injection from electrical contacts, in book Dielectric phenomena in solids. With emphasis on physical concepts of electronic processes – 2004. – P. 327-380. Academic Press. Elsevier Inc. UK. London. https://doi.org/10.1016/B978-012396561-5/50016-5

6. Markku T. Petzold M., Teruaki Motooka. Handbook of silicon based MEMS materials and technologies. // A volume in micro and nano technologies. Third Edition 2020 Elsevier Inc. UK. London. https://doi.org/10.1016/C2018-0-01845-9

7. Meng J., Lee Ch., Li Zh. Adjustment methods of Schottky barrier height in one- and two-dimensional semiconductor devices // Science Bulletin. – 2024. – Vol.69. – P. 1342-1352. https://doi.org/10.1016/j.scib.2024.03.003

8. Divya S., Kallatt S., Chenniappan V., Nair S., Gupta G., Kiran J. Karmakar D., Majumdar K. Nature of carrier injection in metal/2D-semiconductor interface and its implications for the limits of contact resistance // Phys. Rev. B. -Vol. 96. -P. 205423. https://doi.org/10.1103/PhysRevB.96.205423

9. Fauveau A., Martel B., Veirman J., Dubois S., Kaminski-Cachopo A., Ducroquet F. Comparison of characterization techniques for measurements of doping concentrations in compensated n-type silicon // Energy Procedia. – 2016. -Vol. 92. – P. 691-696. https://doi.org/10.1016/j.egypro.2016.07.045

10. Zhang W.J., Chen J.S., Li S., Wu Y.H., Zhang P.L., Yu Z.S., Yue Z.H., Chun Y., Lu H. Electronic and mechanical properties of monocrystalline silicon doped with trace content of N or P: A first-principles study // Solid State Sciences. – 2021. – Vol. 120. – P. 106723. https://doi.org/10.1016/j.solidstatesciences.2021.106723

11. Lee M. Doped silicon's challenging behaviour // Nature Physics. – 2023. – Vol. 19. -P. 614–615. https://doi.org/10.1038/s41567-022-01918-z

12. Nasriddinov S.S., Esbergenov D.M. A Study of complex defect formation in silicon doped with nickel // Russ. Phys. J. – 2023. – Vol. 65. -P. 1559–1563. https://doi.org/10.1007/s11182-023-02801-x

13. Zhang X., Brynda M., Britt R.D., Carroll E.C., Larsen D.S., Louie A.Y., Kauzlarich S.M. Synthesis and characterization of manganese-doped silicon nanoparticles: Bifunctional paramagnetic-optical manomaterial // J. Am. Chem. Soc. – 2007. -Vol. 129. – P. 10668–10669. https://doi.org/10.1021/ja074144q

14. Neumann F., Genenko Y. A., Melzer C., von Seggern H. Self-consistent theory of unipolar charge-carrier injection in metal/insulator/metal systems // J. Appl. Phys. – 2006. -Vol. 100. -P. 084511. https://doi.org/10.48550/arXiv.0704.2322

15. Koehler M., Biaggio I.. Influence of diffusion, trapping, and state filling on charge injection and transport in organic insulators // Phys. Rev. B. – 2003. – Vol. 68. – P. 075205. https://doi.org/10.1103/PhysRevB.68.075205

16. Chen Y., Wang Y., Wang Z. et al. Unipolar barrier photodetectors based on van der Waals heterostructures // Nat Electron. – 2021. – Vol.4. – P. 357–363. https://doi.org/10.1038/s41928-021-00586-w

17. Zhang Q., Li N., Zhang T. et al. Enhanced gain and detectivity of unipolar barrier solar blind avalanche photodetector via lattice and band engineering // Nat Commun. – 2023. – Vol. 14. – P. 418. https://doi.org/10.1038/s41467-023-36117-8

18. Mussabek G., Mirgorodskij I., Kharin A., Taurbayev T., Timoshenko V. Formation and optical properties of nanocomposite based on silicon nanocrystals in polymer matrix for solar cell coating // Journal of Nanoelectronics and Optoelectronics. – 2015. – Vol. 9(6). – P. 738–740. https://doi.org/10.1166/jno.2014.1670

19. Talkenberg F., Illhardt S., Zoltán Radnoczi G., Béla P., Schmidl G., Schleusener A.,Dikhanbayev K., Mussabek G., Gudovskikh A., Sivakov V. Atomic layer deposition precursor step repetition and surface plasma pretreatment influence on semiconductor–insulator–semiconductor heterojunction solar cell // Journal of Vacuum Science and Technology A (JVS A). – 2015. -Vol. 33. -P. 041101-1-5. https://doi.org/10.1116/1.4921726

20. Markhabayeva A.A., Dupre R., Nemkayeva R., Nuraje N. Synthesis of hierarchical WO_3 microspheres for photoelectrochemical water splitting application // Physical Sciences and Technology. – 2023. – Vol. 10(3-4). – P.33-39. https://doi.org/10.26577/phst.2023.v10.i2.04

21. Mussabek G.K., Yermukhamed D., Dikhanbayev K.K., Mathur S., Sivakov V.A. Self-organization growth of Ge-nanocolums // Materials Research Express. – 2017. – Vol. 4. – P. 035003. https://doi.org/10.1088/2053-1591/aa5ed6

22. Tsukuda M., Imaki H., Omura I. Ultrafast lateral 600 V silicon SOI PiN diode with geometric traps for preventing waveform oscillation // Solid-State Electronics. – 2014. -Vol. 104. – P. 61-69. https://doi.org/10.1016/j.sse.2014.11.011

23. Razak N. H. A., Amin N. et al. Influence of pulsed Nd:YAG laser oscillation energy on silicon wafer texturing for enhanced absorption in photovoltaic cells // Results in Physics. – 2023. – Vol.48. – P.106435, https://doi.org/10.1016/j.rinp.2023.106435

24. Liu F., Cheng Y., Yang F., Chen X.. Quantum conductance oscillation in linear monatomic silicon chains // Physica E: Low-dimensional Systems and Nanostructures. – 2014. – Vol. 56. – P. 96-101. https://doi.org/10.1016/j.physe.2013.08.029

25. Patzauer M., Hueck R., Tosolini A., Schönleber K., Krischer K. Autonomous oscillations and pattern formation with zero external resistance during silicon electrodissolutio // Electrochimica Acta. – 2017. – Vol. 246. – P. 315-321. https://doi.org/10.1016/j.electacta.2017.06.005

Information about authors:

Kutub Ayupov, doctor of science, professor at the Tashkent State Technical University (Tashkent, Republic of Uzbekistan) e-mail:ksayupov@gmail.com

Hayrulla F. Zikrillaev, doctor of science, professor at the Tashkent State Technical University (Tashkent, Republic of Uzbekistan) e-mail: zikrillayev_khayrulla@tdtu.uz

Elyor Saitov, PhD, associate professor at the Tashkent University for Applied Sciences, (Tashkent, Uzbekistan), e-mail: elyor.saitov@utas.uz

Nigora Abdullaeva, associate professor at the Tashkent Medical Academy (Tashkent, Uzbekistan), e-mail abnigorka@gmail.com

Zabarjad Umarkhojayeva, Senior lecturer at the Tashkent State Technical University (Tashkent, Uzbekistan), e-mail: zabarjad.umarxojayeva@tdtu.uz

Mirafzal Yakhyayev, PhD, Senior lecturer at the Tashkent State Technical University (Tashkent, Uzbekistan), e-mail: radiaretv@gmail.com